First-principles study of the effect of pressure on the five zirconia polymorphs. II. Static dielectric properties and Raman spectra

Giuseppe Fadda,[1,2,*] Giovanni Zanzotto,[1,†] and Luciano Colombo[2,‡]

[1]*Dipartimento di Metodi e Modelli Matematici per le Scienze Applicate, Università degli Studi di Padova, Via Trieste, 63, I-35121 Padova (PD), Italy*

[2]*Dipartimento di Fisica, Università degli Studi di Cagliari-Cittadella Universitaria, I-09042 Monserrato (Cagliari), Italy*

(Received 19 April 2010; published 17 August 2010)

The structural parameters and phonon spectra of the five known polymorphs of zirconia are computed for pressures up to 48 GPa with density-functional perturbation theory within both the local-density and the generalized-gradient approximations. Thermoelastic properties in the quasiharmonic approximation, including Grüneisen mode parameters (Part I), and dielectric properties, including the lattice contribution and the Raman spectra (Part II) are derived from the phonon calculations and compared to results of experiments and previous computations.

DOI: 10.1103/PhysRevB.82.064106 PACS number(s): 77.22.Ch, 78.30.−j

I. INTRODUCTION

The present paper is the second part (referred to as Part II in the following) of a study of the vibrational, thermoelastic, and dielectric properties of zirconium dioxide ZrO_2 (zirconia) through density-functional perturbation theory within the local-density approximation (LDA) and generalized-gradient approximations (GGA). In the first part[1] (hereafter called Part I) we have presented the computational framework for both Parts, as well as the phonon dispersion curves of the five known polymorphs of ZrO_2, together with some of their thermoelastic properties deduced in the quasiharmonic approximation. The present Part II is devoted to the derived computation of the static dielectric properties, including the Raman spectra, of the five zirconia phases under varying hydrostatic pressure.

Apart for the many technological applications (see Part I) benefiting from its thermomechanical and chemical properties, zirconia is an interesting material also for its possible applications in the semiconductor industry (see Ref. 2 and references therein); however, disappointingly low values of the components of the dielectric tensor were found for the only naturally stable polymorph (the monoclinic phase).

First-principles studies[3–7] have therefore been conducted on the dielectric constants of the cubic and the tetragonal polymorphs (for $p=0$), showing an increase by a factor of 2 of the components of the lattice contribution to the dielectric tensor. Here we reassess these previous investigations, under varying pressure up to 48 GPa, covering also the two remaining polymorphs, i.e., the two orthorhombic high-pressure phases, in order to ascertain whether they have any remarkable dielectric properties. We find that they are indeed better, but marginally so, than those of the monoclinic structure.

After presenting some preliminaries in Sec. II, the computed dielectric properties of each ZrO_2 polymorph in turn are given in Sec. III, for pressure $p=0$, and then under varying p. The Raman spectra of the tetragonal, monoclinic, and of the two orthorhombic phases are given next (Sec. IV). Some conclusive remarks are made in Sec. V.

II. THEORETICAL CONSIDERATIONS

A. Symmetry considerations

Both the dielectric permittivity ϵ (a bulk property of the whole crystal) and the Born effective charges Z^{eff} (a property which depends on the site symmetry) are tensors of rank 2; therefore, they are both invariant under the inversion $\bar{1}$, even if the latter is lacking from the point group P of the crystal or the site-symmetry group S_j of the orbit j. Consequently, the symmetry group of both tensors are the Laue groups corresponding to P or S_j.

As the five investigated polymorphs are all centrosymmetric, the dielectric tensor has P as invariance group; however, some site-symmetry groups S_j are not centrosymmetric (this happens for instance for all orbits of the monoclinic phase). Furthermore, as the Laue group L_j corresponding to S_j may be a proper subgroup of P of index $[P:L_j] \geq 1$, it may happen that there exist $[P:L_j]$ different variants of the tensor of the Born effective charges, related by symmetry operations of P not belonging to L_j.

For instance, the Born effective charges for the Zr orbit $4e$ (site symmetry 1, Laue group $\bar{1}$) of the monoclinic phase are of two (the index of $\bar{1}$ in $2/m$) variants

$$Z_1^{\mathrm{eff}}(\mathrm{Zr,LDA}) = \begin{pmatrix} 5.505 & -0.4476 & 0.2366 \\ -0.1172 & 5.527 & 0.1647 \\ 0.2422 & 0.3975 & 4.865 \end{pmatrix},$$

$$Z_2^{\mathrm{eff}}(\mathrm{Zr,LDA}) = \begin{pmatrix} 5.505 & 0.4476 & 0.2366 \\ 0.1172 & 5.527 & -0.1647 \\ 0.2422 & -0.3975 & 4.865 \end{pmatrix}$$

the second matrix being obtained by acting on the first with the twofold rotation around the $[010]_m$ axis or equivalently with the reflection about the $(010)_m$ plane. The charge neutrality is ensured for the matrix elements which, by invariance with respect to the point group P of the crystal, are absent; in the example above the (1,2), (2,1), (2,3), and (3,2) components cancel out for each orbit separately. The other elements should cancel out when taking into account all or-

TABLE I. Symmetry properties of the five polymorphs of zirconia; the space group is indicated on the left with the corresponding point group between brackets, the crystallographic orbits with the atomic species and Wyckoff position (Ref. 8) in the middle, and the oriented site-symmetry group (with the corresponding Laue group if different) on the right column.

Phase	Orbit	Site symmetry (Laue)
Cubic $Fm\bar{3}m$ ($m\bar{3}m$)	Zr, 4*a*	$m\bar{3}m$
	O, 8*c*	$\bar{4}3m$ ($m\bar{3}m$)
Tetragonal $P4_2/nmc$ ($4/mmm$) (origin choice 2)	Zr, 2*a*	$\bar{4}m2$ ($4/mmm$)
	O, 4*d*	$2mm$ (mmm)
Monoclinic $P2_1/c$ ($2/m$)	Zr/O/O, 4*e*	1 ($\bar{1}$)
Orthorhombic *Pbca* (*mmm*)	Zr/O/O, 8*c*	1 ($\bar{1}$)
Orthorhombic *Pnma* (*mmm*)	Zr/O/O, 4*c*	*m* ($2/m$)

bits; this is however not always strictly true computationally, as seen below. In the following, only one tensor of Born effective charges is given for each orbit; details on symmetry are shown in Table I.

B. Electronic and lattice dielectric tensors; Born effective charges

The *electronic* contribution ϵ^{∞} to the dielectric tensor and the Born effective charges Z^{eff} can be computed using the formalism described in Refs. 9–11. Let $D(\mathbf{0})$ be the dynamical matrix at the Γ point; the *lattice* contribution to the dielectric tensor, resulting from the ionic displacements, is given by

$$\epsilon_{ij}^{\text{lattice}}(\nu) = \frac{4\pi}{V_0} \sum_m \frac{S_{m,ij}}{\nu_m^2 - \nu^2}, \tag{1}$$

[see, for instance, Eq. (52) in Ref. 9], where V_0 is the volume of the primitive cell, ν_m and $S_{m,ij}$ the frequency and mode-oscillator strength of the mth infrared-active eigenmode of $D(\mathbf{0})$, and

$$S_{m,ij} = \sum_{Ik} \frac{1}{\sqrt{M_I}} Z_{I,ik}^{\text{eff}} u_{I,k}^*(m,\mathbf{0}) \times \sum_{Jl} \frac{1}{\sqrt{M_J}} Z_{J,jl}^{\text{eff}} u_{J,l}(m,\mathbf{0}), \tag{2}$$

where $Z_{I,ik}^{\text{eff}}$ is the (i,k) component of the Born effective charge for ion I, $u_{I,k}(m,\mathbf{0})$ the kth component of the mth eigenvector of $D(\mathbf{0})$ corresponding to ion I; * indicates the complex conjugate, and M_I the mass of ion I. The eigendisplacements are normalized according to

$$\sum_{Ii} u_{I,i}^*(m,\mathbf{0}) u_{I,i}(n,\mathbf{0}) = \delta_{mn}$$

δ_{ij} being the identity matrix. The total dielectric tensor is then the sum of the electronic and lattice contributions (no polar contributions exist here as ZrO_2 has no permanent dipole moment, all polymorphs being centrosymmetric). In the following we shall use the shorthand notation $\epsilon_{ij}^{\text{lattice}}$ for the static contribution (i.e., at $\nu=0$).

C. Frequencies at the Γ point

Frequencies (wave numbers) at the Γ point and the corresponding irreducible representations in the Mulliken notation[12] are tabulated below; as is well known, the infrared-active modes transform exactly as the irreducible representations of a polar vector, the induced dipole moment (*ungerade* representations), whereas the Raman-active modes transform as the irreducible representations of a rank-2 symmetric tensor, the Raman polarization tensor (*gerade* representations). Knowing for each eigenmode m the eigenvectors $u(m,\mathbf{0})$ enables to determine the symmetry assignment. In the following, we have indicated the LO-TO splitting for the cubic and tetragonal cases only, as the frequencies of (quasi-) longitudinal waves are direction-dependent, except for waves propagating along symmetry axes and waves traveling in planes orthogonal to a threefold, fourfold, or sixfold axis (see, for instance, Refs. 13 and 14).

D. Pressure dependence of the dielectric properties

Covalent compounds, for which the bond polarizability depends critically on their length, have their electronic dielectric permittivity decrease with the bond length as pressure increases (see for instance Ref. 15 and references therein); on the contrary, for ionic compounds with large band gaps, the density of polarizable centers ρ increases with pressure (as for any other compound), while the microscopic polarizability α remains almost constant (see for instance Refs. 15–17). The pressure dependence of the *electronic* contribution can be found with a simple model using the following local-field equation[15]

$$4\pi\gamma\rho\alpha = \frac{\epsilon^{\infty} - 1}{\epsilon^{\infty} + \frac{1}{\gamma} - 1}, \tag{3}$$

where the dimensionless parameter $\gamma \geq 0$ is a phenomenological constant expressing how sharply the polarization centers are localized: it ranges from 0 (delocalized polarization centers, appropriate for metals, but also for electrons in covalent bonding because of the large overlap of the orbitals forming the bond[15]) to 1/3 (point charges, appropriate for

TABLE II. Electronic contribution ϵ^{∞} to the dielectric permittivity tensor and Born effective charges Z^{eff} for the known polymorphs of zirconia at $p=0$; computations for both sets have been done with $E_{\mathrm{cut}}=15$ Ha. The left column gives the component of the matrices and "–" indicates a zero entry. Oxygen orbits are ordered as in Table I, Part I.

	$Fm\bar{3}m$		$P4_2/nmc$		$P2_1/c$		$Pbca$		$Pnma$	
ϵ^{∞}	GGA	LDA	GGA	LDA	GGA	LDA	GGA	LDA	GGA	LDA
11	5.798	5.746	5.750	5.762	5.350	5.386	5.705	5.683	6.387	6.227
13,31	–	–	–	–	0.1582	0.1735	–	–	–	–
22	5.798	5.746	5.750	5.762	5.386	5.453	5.546	5.523	6.142	6.083
33	5.798	5.746	5.004	5.238	5.027	5.037	5.351	5.358	6.294	6.257
Z^{eff}(Zr)	GGA	LDA	GGA	LDA	GGA	LDA	GGA	LDA	GGA	LDA
11	5.694	5.710	5.745	5.726	5.519	5.505	5.705	5. 664	5.206	5.022
12	–	–	–	–	−0.3828	−0.4476	−0.4327	−0.4277	–	–
13	–	–	–	–	0.2185	0.2366	0.04679	0.04901	0.03575	0.1164
21	–	–	–	–	−0.1851	−0.1172	0.03391	0.01910	–	–
22	5.694	5.710	5.745	5.726	5.444	5.527	5.431	5.453	5.011	4.998
23	–	–	–	–	0.1731	0.1647	0.1440	0.1332	–	–
31	–	–	–	–	0.2770	0.2422	0.3265	0.3101	0.04043	0.1925
32	–	–	–	–	0.3561	0.3975	0.06485	0.03448	–	–
33	5.694	5.710	4.744	5.078	4.890	4.865	5.023	5.062	5.134	5.176
Z^{eff}(O)	GGA	LDA	GGA	LDA	GGA	LDA	GGA	LDA	GGA	LDA
11	−2.827	−2.849	−3.750	−3.529	−3.010	−3.051	−3.064	−3.072	−2.670	−2.632
12	–	–	–	–	1.208	1.144	0.8903	0.8634	–	–
13	–	–	–	–	−0.2017	−0.2129	0.6998	0.6726	−0.1269	−0.03364
21	–	–	–	–	1.458	1.435	1.137	1.092	–	–
22	−2.827	−2.849	−1.979	−2.203	−2.687	−2.719	−2.636	−2.641	−2.647	−2.641
23	–	–	–	–	−0.6914	−0.6599	0.3394	0.3463	–	–
31	–	–	–	–	−0.1894	−0.2030	0.6692	0.6431	−0.00042	0.08638
32	–	–	–	–	−0.7407	−0.6683	0.3460	0.3451	–	–
33	−2.827	−2.849	−2.362	−2.538	−2.302	−2.271	−2.467	−2.494	−2.337	−2.343
Z^{eff}(O)					GGA	LDA	GGA	LDA	GGA	LDA
11					−2.437	−2.454	−2.570	−2.593	−2.465	−2.392
12					0.2421	0.1313	−0.05550	−0.04719	–	–
13					−0.01678	−0.02372	0.1270	0.1102	0.2308	0.2041
21					0.2763	0.1850	−0.01842	−0.01450	–	–
22					−2.740	−2.809	−2.780	−2.814	−2.344	−2.349
23					0.3895	0.3906	0.3008	0.3113	–	–
31					−0.03126	−0.03920	0.01601	0.01542	0.2207	0.2369
32					0.3992	0.4246	0.3449	0.3637	–	–
33					−2.570	−2.596	−2.540	−2.568	−2.781	−2.836

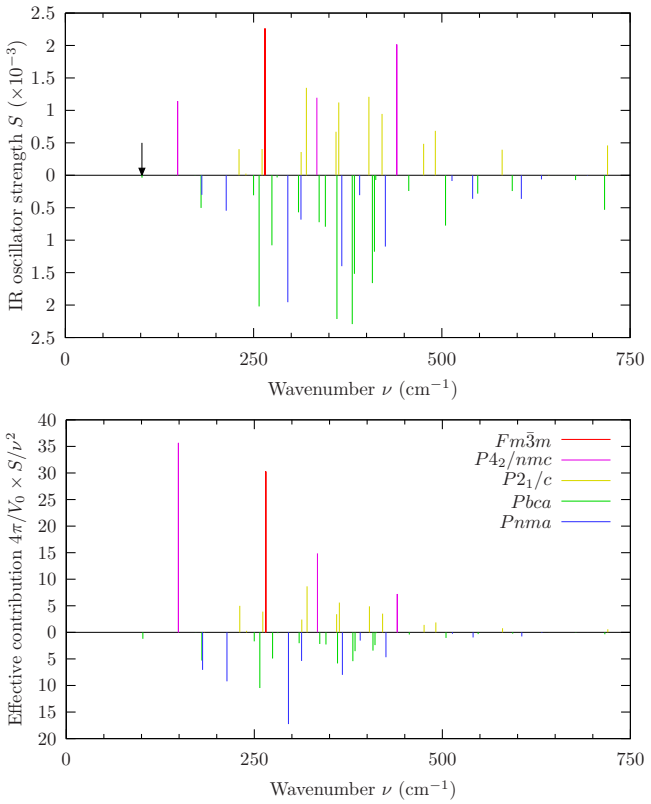

FIG. 1. (Color online) Infrared oscillator strengths, Eq. (2) (top panel) and effective contribution, Eq. (1) (bottom panel), in atomic units, for the five polymorphs of zirconia (LDA). Degeneracy is taken into account for the oscillator strengths. Data on two orthorhombic phases are drawn on the lower part for clarity. The arrow indicates to the lowest *Pbca* mode, which is barely visible at this scale (strength inferior to 4×10^{-5}).

ionic crystals). The latter case gives the well-known Clausius-Mossotti equation (also called Lorentz-Lorenz equation if we replace ϵ^∞ by n^2, where n is the refractive index)

TABLE IV. Pressure and volume dependence of the electronic and lattice contributions to the dielectric tensor of the cubic phase.

p (GPa)	V (au^3/atom)	ϵ_{11}^{∞}	$\epsilon_{11}^{\text{lattice}}$
−23.55	79.78	5.905	121.8
−12.00	75.09	5.805	46.34
−7.997	73.78	5.781	39.05
−3.980	72.58	5.762	34.00
0.051	71.47	5.746	30.28
2.000	70.96	5.739	28.81
4.091	70.43	5.732	27.41
6.001	69.97	5.727	26.26
8.139	69.47	5.721	25.14
12.20	68.57	5.712	23.28
24.20	66.21	5.693	19.40
30.00	65.20	5.688	18.06
33.00	64.71	5.686	17.46
36.36	64.17	5.684	16.84
48.53	62.40	5.683	15.04

$$\frac{4\pi}{3}\rho\alpha = \frac{\epsilon^\infty - 1}{\epsilon^\infty + 2}. \tag{4}$$

Equations (3) and (4) are strictly valid for cubic crystallographic sites only.[18] The pressure derivative of Eq. (3) gives, $\kappa_0 = 1/B_0 = -(\partial \ln V/\partial p)_0$ being the compressibility for the reference state at $p=0$

$$\frac{\partial \ln \epsilon^\infty}{\partial p} = \frac{\epsilon^\infty - 1}{\epsilon^\infty}[\gamma(\epsilon^\infty - 1) + 1] \times \left(\kappa + \frac{\partial \ln \alpha}{\partial p}\right)_0.$$

The electronic dielectric permittivity thus increases with p for ionic compounds (as α remains nearly constant) whereas it decreases beyond a certain critical value $(\partial \ln \alpha/\partial p)_c = -\kappa$ for covalent compounds; as we shall see in Sec. III, zirconia exhibits the two behaviors.

TABLE III. Wave numbers (in cm^{-1}) at $p=0$ of the phonon modes at the Γ point and symmetry assignment for the cubic phase. The first two columns of results (GGA and LDA) refer to the present work, see text. The correspondence has been made on symmetry assignments as given by the authors of the cited works. "Exp" indicates experimental data; the amount of dopants (if any) is indicated with the reference.

Infrared	GGA	LDA	LDA[a]	LDA[b]	Exp[c]	Exp[d]
T_{1u} (TO)	222.1	265.1	258	269.4	358	320
(LO)	629.1	663.9			689	705
Raman	**GGA**	**LDA**	**LDA[b]**	**Exp[e,f]**	**Exp[g]**	**Exp[h]**
T_{2g}	548.0	581.4	587.0	600	614.3	598.5

[a]Reference 21.
[b]Reference 3.
[c]Reference 23 (Y_2O_3 at 46% mol).
[d]Reference 24 (Y_2O_3 at 20% mol).
[e]Reference 25 (Y_2O_3 at 10% mol).
[f]Reference 26 (Y_2O_3 at 20% mol).
[g]Reference 27 (Y_2O_3 at 9.5% mol).
[h]Reference 27 (CaO at 12% mol).

TABLE V. Wave numbers (in cm^{-1}) of the phonon modes and symmetry assignment for the tetragonal phase. See the caption to Table III.

Infrared	GGA	LDA	GGA[a]	LDA[b]	LDA[c]	Exp[d]		
A_{2u} (TO)	320.3	333.5	325	338.5	334	339		
(LO)	609.4	653.7		663.8		354		
E_u (TO)	79.37	148.3	76	152.7	154	164		
(LO)	206.8	261.9		270.5		232		
E_u (TO)	426.6	439.6	435	449.4	437	467		
(LO)	716.3	725.8		734.1		650		
Raman	**GGA**	**LDA**	**GGA[a]**	**LDA[b]**	**Exp[e]**	**Exp[f]**	**Exp[g]**	**Exp[h]**
A_{1g}	300.1	264.8	290	259.1	270	269.4	265	260.4
B_{1g}	279.1	323.2	286	330.5	318	319.4	322	327.8
	571.2	598.3	569	607.0	602	602.5	609	609.0
E_g	122.5	144.5	126	146.7	146	149.2	148	150.6
	411.7	464.6	411	473.7	458	461.6	466	468.0
	619.2	647.0	625	659.2	648	648.5	642	642.6
Silent	**GGA**	**LDA**	**LDA[b]**					
B_{2u}	612.7	661.8	673.4					

[a]Reference 5.
[b]Reference 3.
[c]Reference 21.
[d]Reference 23.
[e]Reference 38.
[f]Reference 39.
[g]Reference 40.
[h]Reference 41 (Y_2O_3 at 5% mass).

The *lattice* contribution is dependent instead on the mode-oscillator strength S_i on one hand, which is directly proportional to the Born effective charges and to the ionic eigendisplacements, and on the frequencies ν_i of these modes on the other hand, whose dependence on pressure is given by the Grüneisen parameters γ_i and the bulk modulus $B=-V\partial p/\partial V$ [see Eq. (2), Part I]. The derivative with respect to pressure of the lattice contribution of the ith mode is given

TABLE VI. Pressure and volume dependence of the electronic and lattice contributions to the dielectric tensor of the tetragonal phase.

p (GPa)	V (au^3/atom)	ϵ_{11}^{∞}	ϵ_{33}^{∞}	$\epsilon_{11}^{\text{lattice}}$	$\epsilon_{33}^{\text{lattice}}$
−17.84	82.66	5.741	4.786	20.98	13.04
−11.98	78.18	5.753	4.977	192.5	13.68
−7.956	76.01	5.757	5.079	87.59	14.12
−3.893	74.24	5.760	5.164	56.97	14.51
0.011	72.77	5.762	5.238	43.24	14.88
3.972	71.45	5.766	5.310	35.19	15.28
8.377	70.16	5.768	5.373	29.81	15.56
12.03	69.17	5.773	5.432	26.53	15.95
18.01	67.74	5.779	5.504	22.99	16.27
24.03	66.43	5.790	5.579	20.44	16.74
30.09	65.25	5.802	5.645	18.60	17.15
32.92	64.73	5.808	5.673	17.91	17.31
36.15	64.21	5.810	5.678	17.28	16.92

TABLE VII. Wave numbers (in cm^{-1}) of the phonon modes and symmetry assignment for the monoclinic phase. See the caption to Table III. A mode at 760 cm^{-1} has been assigned to the A_g irreducible representation in Ref. 46 whereas our computations indicate B_g.

Infrared	GGA	LDA	GGA[a]	LDA[b]	Exp[c]	Exp[d]
A_u						104
	165.9	183.8	170	224		180
						192
	230.5	239.7	233	242	235	233
	244.6	261.2	239	305	258	270
	318.6	359.4	325	347		
	379.6	403.1	386	401		415
	464.9	475.7	461	478	434	443
	541.5	580.0	548	571		
	613.0	642.0	610	634	738	740
B_u	206.9	230.7	212	181		
	276.3	313.1	283	253		
	298.0	320.1	303	319	351	360
	330.3	363.1	341	355	373	373
	389.7	420.5	393	414		
	459.7	491.3	464	483	505	515
					580	620
	686.6	720.0	685	711	738	740

Raman	GGA	LDA	GGA[a]	LDA[b]	Exp[e]	Exp[f]
A_g	98.82	116.9	108	103	102	
	163.7	183.2	169	180	179	176
	175.3	193.2	179	190	190	187
	284.9	324.9	293	317	305	300
	320.6	353.9	324	345	348	
	368.1	383.6	371	381		
	451.5	467.8	453	466	476	475
	524.5	552.1	524	548	556	558
	603.4	634.7	605	631	637	635
B_g	159.2	177.5	162	175	179	
	213.1	225.3	216	224	222	220
	306.9	320.7	303	313		333
	317.2	332.1	316	330	334	344
	364.8	390.3	371	382	381	380
	473.3	488.2	473	489	500	510
	514.2	539.9	512	533	534	536
	576.2	610.6	580	601	615	613
	724.1	750.1	719	748		

[a]Reference 5.
[b]Reference 21.
[c]Reference 43.
[d]Reference 44.
[e]Misprints on symmetry assignments?
[f]Reference 45.
[g]Reference 46.

TABLE VIII. Pressure and volume dependence of the electronic and lattice contributions to the dielectric tensor for the monoclinic phase.

p (GPa)	V (au^3/atom)	ϵ_{11}^{∞}	ϵ_{22}^{∞}	ϵ_{33}^{∞}	ϵ_{12}^{∞}	$\epsilon_{11}^{\text{lattice}}$	$\epsilon_{22}^{\text{lattice}}$	$\epsilon_{33}^{\text{lattice}}$	$\epsilon_{12}^{\text{lattice}}$
−15.92	85.04	5.270	5.209	4.986	0.1632	18.99	17.06	15.02	1.275
−11.89	81.76	5.352	5.318	5.058	0.1487	19.40	17.57	14.29	1.134
−7.961	79.94	5.361	5.351	5.053	0.1460	18.24	16.34	12.95	1.124
−3.985	78.31	5.367	5.389	5.042	0.1505	17.28	15.37	11.85	1.043
0	76.60	5.386	5.453	5.037	0.1735	16.66	14.76	10.99	0.9793
4.059	74.54	5.444	5.529	5.061	0.2063	16.12	14.21	10.60	0.9362
8.156	72.47	5.523	5.591	5.106	0.2224	15.57	13.54	10.91	0.8847
12.28	70.51	5.614	5.652	5.163	0.2216	14.91	12.92	12.14	0.7638
18.51	67.00	5.840	5.799	5.312	0.1656	13.77	12.34	42.27	−1.469

by

$$\frac{\partial(S_i/\nu_i^2)}{\partial p} = \frac{1}{\nu_i^2}\left(\frac{\partial S_i}{\partial p} - \frac{2S_i\gamma_i}{B_0}\right) \tag{5}$$

the subscript 0 refers to the reference state at $p=0$. Depending on the variation in the Born effective charges with pressure, the lattice contribution may therefore increase even for modes with positive Grüneisen parameters; however, it is expected in most cases that the second term in Eq. (5) be dominant, hence leading to a decrease in lattice contribution as pressures increases.

III. DIELECTRIC PROPERTIES

A. Electronic contribution and Born effective charges

The results for all the zirconia polymorphs, at $p=0$, are summarized in Table II. The charge neutrality rule is slightly violated, which is a consequence of the truncation of the density of charge when passing from real to Fourier space, especially pronounced when using insufficient Brillouin zone (BZ) sampling, core corrections and GGA ultrasoft potentials.[19]

The prominent features are: (i) rather marked deviations of the Born effective charges with respect to the nominal static ionic charges, showing an important dynamical transfer of charge between the strongly electronegative O^{2-} and the weakly electropositive Zr^{4+} ions;[20,21] (ii) a marked anisotropy of the dielectric and Born charge tensors for the tetragonal, monoclinic, and orthorhombic *Pbca* phase, with a systematic decrease of approximately 10% of the zz component with respect to the other two diagonal terms.

Figure 1 gives explicitly the infrared mode-oscillator strengths [as calculated in Eqs. (1) and (2)] of the five polymorphs, useful in understanding the relative values of the dielectric constants. The bottom panel shows the large effect of the volume V_0 of the primitive cell on the diminution of the effective contribution to the lattice dielectric tensor.

B. Cubic $Fm\bar{3}m$ phase

1. Results at $p=0$

The dielectric tensors and the Born effective charges have cubic symmetry, i.e., they are isotropic. There is good agreement with the computational results obtained in Refs. 21 and 22.

Wave numbers at the Γ point are given in Table III. As explained in Sec. III A, Part I, experimental data are for stabilized zirconia, as cubic zirconia is not stable at room conditions, and structural disorder associated with oxygen vacancies shows clearly in the infrared and Raman spectra; compare Fig. 2 in Ref. 25 with Fig. 3 in Ref. 28; see also Table I in Ref. 23. The decomposition of the vibrational representation Γ_{vib} (see, for instance, Refs. 29 and 30) into irreducible representations at the Γ point is

$$\Gamma_{\text{vib}}(\text{Zr}) = T_{1u},$$

$$\Gamma_{\text{vib}}(\text{O}) = T_{1u} + T_{2g}$$

thus only one triply degenerate mode is infrared active; the Raman mode T_{2g} is entirely due to the oxygen sublattice (Table III).

As we have seen in Part I, the large Grüneisen parameters explain the strong variation of the wave numbers with volume and therefore the softening of phonons when using the generalized-gradient approximation. Given that the frequencies enter Eq. (1) with a square, it is therefore not surprising to see large differences for the lattice contribution, which are found to be

$$\epsilon_{ij}^{\text{lattice}}(\text{GGA}) = 40.72\,\delta_{ij} \quad \text{and} \quad \epsilon_{ij}^{\text{lattice}}(\text{LDA}) = 30.28\,\delta_{ij},$$

respectively, to be compared to $31.8\,\delta_{ij}$ (Ref. 21) and $30.5\,\delta_{ij}$ (Ref. 4). When increasing the cutoff energy to 30 Ha and the BZ sampling to $8\times8\times8$, the GGA value is still seriously overestimated ($\epsilon_{ij}^{\text{lattice}}=41.47\,\delta_{ij}$) with respect to the LDA calculations ($\epsilon_{ij}^{\text{lattice}}=30.33\,\delta_{ij}$ with the same sampling); this is also the case for the tetragonal polymorph as seen below.

TABLE IX. Wave numbers (in cm^{-1}) of the phonon modes and symmetry assignment for the orthorhombic *Pbca* phase. See the caption to Table III.

Infrared	GGA
B_{1u}	174.5, 227.0, 263.0, 303.4, 328.8, 363.2, 507.8, 620.6
B_{2u}	155.6, 237.1, 258.6, 339.7, 376.2, 427.5, 556.0, 643.4
B_{3u}	96.22, 238.1, 270.8, 314.6, 344.6, 376.8, 483.2, 685.0
Raman	**GGA**
A_g	127.9, 166.0, 194.7, 275.2, 315.0, 339.2, 376.9, 515.6, 561.8
B_{1g}	154.4, 201.3, 274.5, 294.3, 395.5, 417.7, 530.9, 598.9, 645.3
B_{2g}	176.9, 218.2, 244.6, 281.9, 296.3, 412.8, 461.6, 528.5, 754.6
B_{3g}	134.5, 166.0, 238.8, 277.6, 327.7, 457.1, 514.5, 566.2, 650.1
Silent	**GGA**
A_u	109.1, 164.2, 187.4, 296.1, 341.8, 385.3, 467.9, 528.8, 682.2
Infrared	**LDA**
B_{1u}	180.2, 250.2, 281.3, 337.0, 360.7, 410.4, 547.6, 650.8
B_{2u}	172.3, 250.0, 274.3, 381.0, 407.7, 456.0, 593.5, 677.3
B_{3u}	101.7, 257.3, 309.7, 345.2, 383.8, 412.2, 504.9, 715.9
Raman	**LDA**
A_g	136.9, 184.4, 204.6, 315.0, 344.1, 359.2, 414.0, 550.0, 599.2
B_{1g}	173.7, 213.8, 285.6, 307.6, 419.6, 443.2, 563.2, 637.9, 676.6
B_{2g}	191.3, 223.8, 261.0, 307.5, 328.2, 442.0, 480.4, 563.2, 789.0
B_{3g}	148.3, 172.7, 261.4, 318.7, 347.0, 474.6, 549.3, 600.9, 685.6
Silent	**LDA**
A_u	117.6, 173.5, 202.4, 309.6, 377.9, 419.6, 493.2, 562.8, 716.7

2. Pressure dependence

The electronic and lattice contributions (see Table IV) decrease with pressure, quite slowly for the first; the cubic phase having a relatively large positive Grüneisen parameter for the infrared-active T_{1u} mode (γ=4.3), the decrease is faster for the lattice contribution.

Data on the refractive index $n=\sqrt{\epsilon^{\infty}}$ are available on yttria-stabilized cubic zirconia;[31] the logarithmic derivative is computed to be $\partial \ln n/\partial p=(-2.676\pm0.102)\times10^{-4}$ GPa^{-1}, which is quite different from the experimentally found value $(-1.0\pm0.5)\times10^{-4}$ GPa^{-1}, both in the same 0–8 GPa range. Doping might be the source of such a divergence (the sample used was doped with 20% mol Y_2O_3).

The decrease with pressure of the electronic contribution can also be estimated through the Mueller parameter

$$\Lambda_0=\left(\frac{\partial \ln \alpha}{\partial \ln V}\right)_T$$

(see Ref. 32); assuming Eq. (4) is valid, the polarizability α can be computed for each volume and a value of $\Lambda_0=1.072\pm0.002$ is found, to be compared to 1.02 ± 0.01 derived in Ref. 31.

C. Tetragonal $P4_2/nmc$ phase

1. Results at $p=0$

The electronic dielectric tensor has tetragonal ($4/mmm$) symmetry; as seen in Table II, there is a distinct anisotropy, as is also the case for the Born effective charges (symmetry $4/mmm$ and mmm for Zr and O, respectively). These anisotropies, observed also for the elastic properties (see, for instance, Refs. 33–37), are especially noticeable when considering the fact that the tetragonal polymorph is but a slight modification of the cubic phase. The present computations are in good agreement with the previous computations in Refs. 21 and 22.

Wave numbers are given in Table V; the softening of the phonons for both GGA computations clearly appears. We have (modes being regrouped according to activity)

$$\Gamma_{\mathrm{vib}}(\mathrm{Zr})=(A_{2u}+E_u)+(B_{1g}+E_g),$$

$$\Gamma_{\mathrm{vib}}(\mathrm{O})=(A_{2u}+2E_u)+(A_{1g}+B_{1g}+2E_g)+B_{2u}$$

the motion of the Zr sublattice is almost entirely responsible of the Raman-active B_{1g} mode at 323.2 cm^{-1} and E_g mode at 144.5 cm^{-1}.

The lattice dielectric tensor is evaluated with the LDA potentials as

$$\epsilon^{\mathrm{lattice}}(\mathrm{LDA})=\begin{pmatrix}43.24 & 0 & 0\\ 0 & 43.24 & 0\\ 0 & 0 & 14.88\end{pmatrix}$$

in excellent agreement with previous computational results[3,21] whereas the GGA computations give

TABLE X. Pressure and volume dependence of the electronic and lattice contributions to the dielectric tensor for the orthorhombic *Pbca* phase.

p (GPa)	V (au^3/atom)	ϵ_{11}^{∞}	ϵ_{22}^{∞}	ϵ_{33}^{∞}	$\epsilon_{11}^{\text{lattice}}$	$\epsilon_{22}^{\text{lattice}}$	$\epsilon_{33}^{\text{lattice}}$
−12.00	77.86	5.706	5.525	5.383	27.26	21.06	19.54
−7.986	76.29	5.696	5.519	5.375	24.76	19.01	18.06
−3.949	74.85	5.688	5.519	5.366	22.76	17.44	16.99
0.1	73.51	5.683	5.523	5.358	21.09	16.18	16.21
4.220	72.25	5.679	5.531	5.352	19.58	15.11	15.51
8.236	71.04	5.684	5.552	5.344	18.40	14.26	15.28
12.31	69.88	5.693	5.574	5.340	17.28	13.51	15.08
16.35	68.75	5.708	5.603	5.337	16.24	12.86	15.07

$$\epsilon^{\text{lattice}}(\text{GGA}) = \begin{pmatrix} 104.4 & 0 & 0 \\ 0 & 104.4 & 0 \\ 0 & 0 & 13.11 \end{pmatrix}.$$

We notice that the GGA grossly overestimates these quantities; increasing the BZ sampling to $8\times8\times8$ and the cut-off energy to 30 Ha does not much change these results, yielding 43.94 and 14.93 (LDA), and 113.6 and 13.47 (GGA) for the (001) and [001] components, respectively. The already large contribution of the E_u mode at 148.3 cm^{-1} (see Fig. 1) is increased nearly fourfold by the GGA, for which this frequency is 79.37 cm^{-1} instead.

Again we observe a marked anisotropy in the lattice dielectric tensor, as we did for the elastic properties. The doubly degenerate mode at 148.3 cm^{-1} (E_u) accounts for 80% of the $\epsilon_{11}^{\text{lattice}}$ component with a contribution similar to the cubic T_{1u} mode (35 against 30, see Fig. 1) whereas the A_{2u} mode is the only responsible of the $\epsilon_{33}^{\text{lattice}}$ component; the lower contribution (one third) of the latter with respect to the E_u modes, in spite of nearly equivalent strengths (see Fig. 1), is caused by the already large frequency.

2. Pressure dependence

As seen in Sec. III B, Part I, the Grüneisen parameters of the infrared-active modes range from a very low value, 0.221 for the highest-frequency E_u (LO) mode, to a very high one, 8.91 for the lowest-frequency E_u (TO) mode. Consequently, the value of the lattice contribution is expected to increase with the equilibrium volume and to decrease (sharply for $\epsilon_{11}^{\text{lattice}}$) with pressure. This is the observed behavior for the latter (see Table VI); on the other hand, the small increase of $\epsilon_{33}^{\text{lattice}}$ with p is to be attributed to a gain in oscillator strength [see Eq. (5) above], which in turn stems from the increase in magnitude of the Z_{33}^{eff} component of the Born effective charge [see Eq. (2)], which follows the same trend than ϵ_{33}^{∞} [see below, and also Fig. 4(b) in Ref. 7].

As can be seen in Table VI, the ϵ_{11}^{∞} component shows little change with p ($\partial \ln n/\partial p = (1.036 \pm 0.050)\times10^{-4}$ GPa^{-1}), whereas ϵ_{33}^{∞} increases with pressure, similarly to the monoclinic phase but in contrast to the cubic phase [$\partial \ln n/\partial p = (1.337 \pm 0.04)\times10^{-3}$ GPa^{-1} in the 0–30 GPa pressure range]. At a pressure of approximately 36 GPa, the tetragonal phase undergoes a transition to the cubic phase (see Ref. 7 and Part I), and consequently the dielectric tensor becomes isotropic; this transition is also apparent in the Raman spectra (Sec. IV).

D. Monoclinic $P2_1/c$ phase

1. Results at $p=0$

The Cartesian axes chosen to represent the dielectric tensor are Ox along $[100]_m$, Oy along $[010]_m$, and Oz orthogonal to both. The electronic dielectric tensor has invariance group $2/m$, whereas the Born effective charges all have invariance group $\bar{1}$. Both tensors are in excellent agreement with those computed in Ref. 21, although the used Cartesian axes are not explicitly indicated there (the monoclinic angle β however is close to $\pi/2$ so the difference between the rotated tensors is small, see below). The monoclinic and tetragonal phases have similar electronic dielectric properties as can be seen in Table II with a strong anisotropy in the [001] direction for both. This similitude is also found for the elastic properties,[37] which would suggest a privileged relationship between the $[001]_t$ and $[001]_m$ directions.

Using Eq. (4) (ionic limit) and taking as dielectric constant the average value of the diagonal terms of the tensor, we find a polarizability of 32.29 a.u.$^3 = 4.785\times10^{-3}$ nm^3, in good agreement with the experimental result of Ref. 42, which gives 4.64×10^{-3} nm^3.

The vibration representation decomposes according to

$$\Gamma_{\text{vib}}(\text{Zr}) = 3(A_u + B_u) + 3(A_g + B_g),$$

$$\Gamma_{\text{vib}}(\text{O}) = 2\Gamma_{\text{vib}}(\text{Zr})$$

as atoms all occupy orbit $4e$; the Zr ions contribute to a large extent to the Raman-active modes between 180 and 225 cm^{-1}, and negligibly to the others. Wave numbers are indicated in Table VII. The agreement with experiment is generally fair, in particular for Raman frequencies. The lattice contribution is computed to be

TABLE XI. Wave numbers (in cm^{-1}) of the phonon modes and symmetry assignment for the orthorhombic *Pnma* phase. See the caption to Table III and the text for the correspondences. A mode at 201 cm^{-1} (indicated as "very very weak" in Ref. 48) could not be assigned.

Infrared	GGA	LDA	
B_{1u}	137.7	181.3	
	280.3	312.8	
	393.7	425.0	
	559.8	605.6	
	609.4	632.3	
B_{2u}	256.5	295.4	
	502.7	540.8	
B_{3u}	177.2	213.6	
	331.4	367.1	
	363.3	390.8	
	482.6	513.5	
	659.6	693.3	
Raman	GGA	LDA	Exp[a]
A_g	150.4	166.8	163
	225.1	242.6	239
	333.5	359.5	362
	415.1	435.7	436
	526.1	566.1	569
	584.5	619.3	622
B_{1g}	152.9	176.2	167
	365.1	374.6	378
	557.9	597.3	
B_{2g}	252.6	286.4	279
	326.0	342.5	341
	363.1	390.7	387
	512.4	542.7	
	538.5	555.0	561
	616.0	662.5	661
B_{3g}	139.1	154.7	149
	395.7	405.4	413
	556.8	602.7	601
Silent	GGA	LDA	
A_u	104.8	120.2	
	293.9	313.1	
	439.1	483.0	

[a]Reference 48.

$$\epsilon^{\text{lattice}}(\text{LDA}) = \begin{pmatrix} 16.66 & 0 & 0.9793 \\ 0 & 14.76 & 0 \\ 0.9793 & 0 & 10.99 \end{pmatrix}$$

in excellent agreement with the computed values in Refs. 6 and 21. The GGA gives instead

$$\epsilon^{\text{lattice}}(\text{GGA}) = \begin{pmatrix} 19.05 & 0 & 1.478 \\ 0 & 16.92 & 0 \\ 1.478 & 0 & 13.00 \end{pmatrix}$$

still overestimated with respect to the LDA.

The absence of strong low-frequency infrared modes is remarkable, especially when compared to the tetragonal phase (see Fig. 1) and results in a lower lattice contribution to the dielectric tensor than for the cubic or tetragonal phases; for instance, the strongest monoclinic mode is at twice the frequency of its tetragonal equivalent, implying a reduced contribution by a factor of $8=4\times2$ (the second factor coming from the ratio of the volumes of the primitive cells); given the symmetry, this mode contributes to the $\epsilon_{11}^{\text{lattice}}$ component, but not to the other diagonal components.

2. Pressure dependence

As can be seen from the results in Table VIII, the electronic contribution increases while the lattice contribution decreases with increasing pressure. There is however a nonmonotonic behavior for the ϵ_{33}^{∞} component, also seen with the *Pbca* phase (see below): the variation is, if we disregard the datum at 18 GPa, rather reduced. The increase with pressure is the expected behavior for predominantly ionic compounds; this was anticipated because the Clausius-Mossotti Eq. (4), valid in the ionic limit, yields a value close to experiment. Data from Ref. 31 give the logarithmic derivative of the refractive indices for a Cartesian basis $\mathcal{B}'=(\vec{c}^*,\vec{b},\vec{c})$; if P is the matrix of the rotation of angle $\beta(p)-\pi/2$ around [010], where $\beta(p)$ is the monoclinic angle which is a function of pressure p, the transformed dielectric tensor in the $\mathcal{B}'$ basis is $\epsilon'=P^{-1}\cdot\epsilon\cdot P$. We have computed $\partial \ln n/\partial p$ for positive values of the pressure (as in the experiment) and found: (i) in the [010] direction, $(1.474\pm0.068)\times10^{-3}$, in serious disagreement with experiment, which gives $(-5.0\pm0.5)\times10^{-4}$ GPa^{-1} and thus a decrease in the refractive index with pressure; (ii) in the $\vec{c}^*$ direction, $(1.355\pm0.115)\times10^{-3}$ GPa^{-1}, in excellent agreement with the experimental value of $(13.5\pm0.5)\times10^{-4}$ GPa^{-1}. The causes of such a dissimilar behavior are not understood. The logarithmic derivative along the [001] direction is found to be $(1.863\pm0.068)\times10^{-3}$ GPa^{-1}. The influence of pressure is tenfold the one observed in the cubic phase.

As mentioned in Part I, computations in the LDA case indicate that the monoclinic phase becomes unstable between 18 and 24 GPa; it can be seen from Table VIII that the $\epsilon_{12}^{\text{lattice}}$ component decreases with pressure and should reach zero between 12 and 18 GPa. At 18 GPa, the lowest infrared-active mode at 121.1 cm^{-1} (compare with its equivalent B_u mode at 230.7 cm^{-1} at $p=0$, see Table VII) is single-handedly responsible for the high value of $\epsilon_{33}^{\text{lattice}}$ and with two other modes of the negative value of $\epsilon_{12}^{\text{lattice}}$.

E. Orthorhombic *Pbca* phase

1. Results at p=0

No experimental or theoretical data are available on this phase. The electronic dielectric tensor (invariance group

TABLE XII. Pressure and volume dependence of the electronic and lattice contributions to the dielectric tensor for the orthorhombic *Pnma* phase.

p (GPa)	V (au^3/atom)	ϵ_{11}^{∞}	ϵ_{22}^{∞}	ϵ_{33}^{∞}	$\epsilon_{11}^{\text{lattice}}$	$\epsilon_{22}^{\text{lattice}}$	$\epsilon_{33}^{\text{lattice}}$
−11.91	68.99	6.348	6.104	6.242	26.19	24.73	26.70
−5.963	67.04	6.280	6.099	6.263	22.14	20.95	21.19
0.007	65.48	6.227	6.083	6.257	19.03	18.22	18.01
6.022	64.12	6.183	6.063	6.246	16.76	16.19	15.86
12.09	62.91	6.148	6.046	6.232	15.06	14.64	14.33
18.17	61.81	6.117	6.030	6.219	13.74	13.42	13.15
24.25	60.81	6.090	6.015	6.207	12.69	12.44	12.21
36.00	59.09	6.048	5.992	6.189	11.15	10.99	10.84
48.00	57.56	6.016	5.974	6.174	10.03	9.916	9.827

mmm) and the Born effective charges (invariance group $\bar{1}$) reported in Table II are found to be similar to those of the tetragonal and monoclinic phases, while slightly less anisotropic.

Wave numbers are given in Table IX. The decomposition of the vibrational representation is

$$\Gamma_{\text{vib}}(\text{Zr}) = 3(B_{1u} + B_{2u} + B_{3u}) + 3(A_g + B_{1g} + B_{2g} + B_{3g}) + 3A_u,$$

$$\Gamma_{\text{vib}}(\text{O}) = 2\Gamma_{\text{vib}}(\text{Zr}).$$

Finally, the lattice contribution to the dielectric tensor is

$$\epsilon^{\text{lattice}}(\text{LDA}) = \begin{pmatrix} 21.09 & 0 & 0 \\ 0 & 16.18 & 0 \\ 0 & 0 & 16.21 \end{pmatrix}$$

somewhat higher than the values obtained for the monoclinic phase. This is explained by the large number of strong infrared modes, as illustrated in Fig. 1, with respect to the monoclinic phase; these modes are however strongly penalized by the volume term in Eq. (1), which explains the relatively modest values of the lattice contribution (compare in Fig. 1 the contributions of two equally strong modes of the *Pbca* and *Pnma* polymorphs). Furthermore, because of low symmetry just as in the monoclinic case, the various modes contribute for one component only; for instance, the mode at 257.3 cm^{-1} accounts for half the $\epsilon_{11}^{\text{lattice}}$ component but for nothing else (Table X).

The GGA result is

$$\epsilon^{\text{lattice}}(\text{GGA}) = \begin{pmatrix} 26.21 & 0 & 0 \\ 0 & 20.01 & 0 \\ 0 & 0 & 18.71 \end{pmatrix}$$

somewhat overestimated.

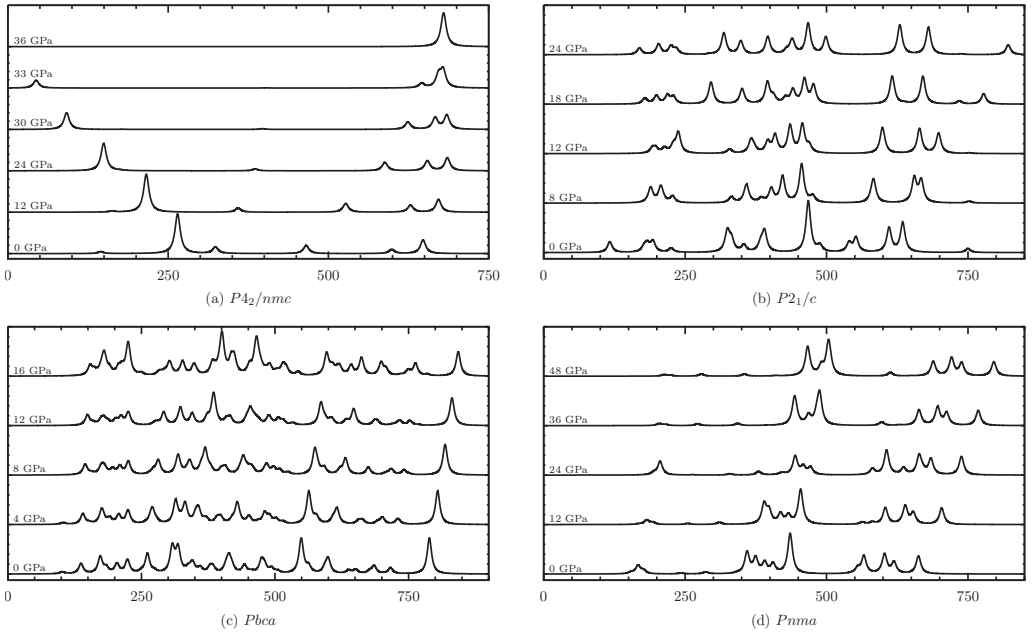

FIG. 2. Variation with pressure (indicated just above each curve on the left) of the computed Raman spectra of the (a) tetragonal, (b) monoclinic, (c) orthorhombic *Pbca*, and (d) orthorhombic *Pnma* phases (LDA). x axis: Raman shift in cm^{-1}, y axis: Raman intensity in arbitrary units. (a) The cubic case is well represented by the curve at 36 GPa of the tetragonal phase.

2. Pressure dependence

The electronic contribution shows a nonmonotonic behavior in the [100] and [010] directions whereas the ϵ_{33}^{∞} component decreases with pressure. As the variation is extremely weak overall, in practice the electronic contribution can be considered to be constant in the studied pressure range.

The anisotropic dependence on pressure of the lattice contribution is explained by the fact that, while a third of the value of the $\epsilon_{33}^{\text{lattice}}$ component comes from the lowest-frequency mode (B_{1u} at 181.3 cm^{-1}), which has a very low Grüneisen parameter (0.277 ± 0.06), all the other contributing modes have higher Grüneisen parameters: for instance the mode at 257.3 cm^{-1} has $\gamma=1.98$ and its contribution is therefore already cut by 25% at 12 GPa.

F. Orthorhombic *Pnma* phase

1. Results at $p=0$

The electronic dielectric tensor has for invariance group *mmm* and is only slightly anisotropic (see Table II) while reaching the highest value for all polymorphs, as predicted by Ref. 47. The Born effective charges (invariance group $2/m$) while also only slightly anisotropic are however in line with the values obtained for the other phases.

The vibration representation is decomposed according to

$$\Gamma_{\text{vib}}(\text{Zr}) = (2B_{1u} + B_{2u} + 2B_{3u}) + (2A_g + B_{1g} + 2B_{2g} + B_{3g}) + A_u,$$

$$\Gamma_{\text{vib}}(\text{O}) = 2\Gamma_{\text{vib}}(\text{Zr})$$

Zr ions contribute for two-thirds of the intensity of the Raman mode at 166.8 cm^{-1}, and very little to the other Raman-active modes. In Table XI the wave numbers are reported, as well as the available experimental result. The correspondence is based on Raman activity and the proximity of the wave number values, as no symmetry assignment was published.

The lattice contribution to the dielectric tensor is then found to be

$$\epsilon^{\text{lattice}}(\text{LDA}) = \begin{pmatrix} 19.03 & 0 & 0 \\ 0 & 18.22 & 0 \\ 0 & 0 & 18.01 \end{pmatrix}$$

similar to the tensor obtained for the orthorhombic *Pbca* phase; the slightly smaller values are essentially a consequence of a shift toward larger frequencies of the strong infrared modes (see Fig. 1); for instance, the mode at 295.4 cm^{-1} is the first (in order of increasing frequencies) to contribute to the $\epsilon_{yy}^{\text{lattice}}$ component (Table XII).

The GGA value is again overestimated

$$\epsilon^{\text{lattice}}(\text{GGA}) = \begin{pmatrix} 25.26 & 0 & 0 \\ 0 & 23.62 & 0 \\ 0 & 0 & 24.59 \end{pmatrix}.$$

2. Pressure dependence

The electronic contribution decreases with applied pressure, which indicates that the *Pnma* phase behaves more as a covalent than as a ionic compound: this is consistent with its higher bulk modulus. The logarithmic derivatives of the refractive indices are, for the three [100], [010], and [001] directions, -4.794 ± 0.157, -2.380 ± 0.048, and -1.652 ± 0.018 (all figures in 10^{-4} GPa^{-1}), respectively, exhibiting a stronger anisotropy than hinted at when comparing the refractive indices themselves.

IV. RAMAN SPECTRA

The Raman spectra can be deduced from the derivatives (here calculated by finite differences) with respect to atomic displacements of the electronic dielectric tensor; see Refs. 49 and 50 and references therein for details. The spectra are computed using (i) the Raman intensities which are proportional to S_i/ν_i, where S_i is the scattering activity coefficient and ν_i the frequency of the mode i, (ii) a Lorentzian broadening of 5 cm^{-1}, and (iii) a temperature of 1 K for the photon occupation number. In this Section, γ_i stands for the value of the Grüneisen parameter of mode i.

The cubic case is the simplest, as there is only one Raman-active mode (T_{2g}, $\gamma_i=1.5$); the curve at 36 GPa in Fig. 2(a) is representative of the shape of the Raman spectra at various pressures. Published Raman spectra are for stabilized samples only;[25–27] we have already insisted on the noticeable effects such a doping can have on the infrared and Raman spectra, making comparisons with experiments rather difficult.

The case of the tetragonal polymorph has been treated extensively in Refs. 7 and 39; the present computations are in agreement with both [see Fig. 2(a)]. The already discussed redshift of the A_{1g} mode (the strong peak to the left, for which $\gamma_i=-2.5$) appears clearly, as well as the reduction of its intensity with increasing pressure, until its total disappearance. On the contrary, we can see the blueshift of the B_{1g} and E_g modes (the three peaks to the right, all with positive γ_i) with a larger intensity and progressively merging as pressure is increased. At 36 GPa, the transition to the cubic phase is complete and a unique peak is left at 680 cm^{-1}, which is exactly the computed frequency of the cubic T_{2g} mode at that pressure.

The three remaining phases exhibit more complex spectra because of the larger number of atoms in their primitive cells. The monoclinic spectrum at $p=0$ [Fig. 2(b)] is in agreement with the published experimental data;[51–54] the most intense peak corresponds to the A_g mode at 467.8 cm^{-1} (experimental data give a range of 463–476 cm^{-1}). The spectrum changes with pressure according to the interactions of modes having different Grüneisen parameters; however, contrary to the orthorhombic polymorphs, the monoclinic phase is characterized by modes with a nonmonotonic dependence on pressure (the B_g mode at 320.7 cm^{-1} is an example) which complicates the interpretation of the spectra.

No experimental data are available for the orthorhombic *Pbca* phase. The Raman spectra are characterized by the large number of active modes, the most intense being the

A_g-B_{1g}-B_{2g}-B_{3g} set at around 300 cm^{-1}, the B_{3g} mode at 550 cm^{-1} and the B_{2g} mode at 789 cm^{-1}; the first set seems to become the most prominent as pressure increases.

The spectrum of the orthorhombic *Pnma* phase [see Fig. 2(d)] is in good agreement with the experimental data[48] except for the intensity of the mode at 167 cm^{-1} which is underestimated by a factor of 4 with respect to the experimental result (see their Fig. 4); the dependence on the photon temperature however significantly affects the value of this peak. The most intense mode is correctly assigned at 436 cm^{-1} (A_g mode), which can be followed up to 48 GPa: at 24 GPa it interacts strongly with its neighbors which, having larger values of γ_i (1.3–1.7 against 1 for the A_g mode), have a stronger dependence on pressure (they "travel faster"). The high-frequency modes form a relatively coherent group as they all have similar γ_i (about 1.5) and thus "travel together" without interaction. The other modes have very different γ_i and thus merge and interact strongly, then separate again as pressure is further increased.

V. CONCLUSIONS

We have investigated the dielectric properties of the five known zirconia polymorphs under pressure through density-functional perturbation theory. The electronic contribution to ϵ is found to be comparable in all these structures with a somewhat higher contribution in the orthorhombic *Pnma* polymorph.[47] The agreement with the available experimental data on refractive indices[31] for the monoclinic case is contrasting.

On the other hand, as expected, the lattice contribution to ϵ is found to depend rather markedly on the structure. Because of the generally large values of the Grüneisen parameters for the five polymorphs, the GGA is found to be inappropriate. Indeed, due to its overestimate of equilibrium volumes, the GGA systematically underestimates the phonon frequencies, and thus overestimates the value of the dielectric constants. The more reliable computations of the dielectric properties are therefore those performed in the LDA, which are in very good agreement with previous computations (all done in the LDA, and with $p=0$) and available experimental data on infrared- and Raman-active modes. The cubic and tetragonal phases, because of their high symmetry, have degenerate modes which add to the same components of the lattice contribution to ϵ; thus a single mode can be very efficient in increasing the dielectric constants (see Fig. 1), aided in this by the relatively small volumes of the primitive cells of these polymorphs.

On the contrary, owing to their lower symmetry there are no such degenerate modes in the monoclinic and orthorhombic phases: a single mode generally contributes to a single component of ϵ only, and the primitive cells are furthermore comparatively larger, having four or eight times the volume of their cubic counterpart. The case is clearly illustrated by the two orthorhombic polymorphs in Fig. 1: the *Pbca* phase has more modes with higher oscillator strength than the *Pnma* polymorph but their effective contributions are cut in half by the fact that the primitive cell of the former is twice as big as that of the latter. The monoclinic phase suffers at the same time of a lack of low-frequency modes, of a relative mode weakness, and of a volume effect: its lattice contribution is therefore the lowest of all polymorphs. Altogether, we find none of the monoclinic and orthorhombic phases to have comparable values of the dielectric constants to those in the cubic and tetragonal structures.

An interesting observation is that both the cubic and tetragonal phases exhibit low-energy modes, and high dielectric constants, in the (001) plane, having at the same time the corresponding C_{66} modulus ($=C_{44}$ in the cubic case) approximately half that of the other three polymorphs.[37] There is likely a connection between these two properties; however, a better understanding of such the complex interplay among elastic, vibrational, electronic, and dielectric properties requires a detailed analysis which is beyond the scope of the present work.

ACKNOWLEDGMENTS

We acknowledge the partial support of the MATHMAT and MATHXPRE Projects of the Università di Padova, Italy. The computations were done on the cluster of the Cybersar Consortium, Cagliari, Italy.

*fadda@dsf.unica.it
†zanzotto@dmsa.unipd.it
‡luciano.colombo@dsf.unica.it

[1] G. Fadda, G. Zanzotto, and L. Colombo, preceding paper, Phys. Rev. B **82**, 064105 (2010).
[2] *The International Technology Roadmap for Semiconductors* (Semiconductor Industry Association, 2001).
[3] G.-M. Rignanese, F. Detraux, X. Gonze, and A. Pasquarello, Phys. Rev. B **64**, 134301 (2001).
[4] V. Fiorentini and G. Gulleri, Phys. Rev. Lett. **89**, 266101 (2002).
[5] A. Kuwabara, T. Tohei, T. Yamamoto, and I. Tanaka, Phys. Rev. B **71**, 064301 (2005).
[6] G. Dutta, K. P. S. S. Hembram, G. M. Rao, and U. V. Waghmare, Appl. Phys. Lett. **89**, 202904 (2006).
[7] V. Milman, A. Perlov, K. Refson, S. J. Clark, J. Gavartin, and B. Winkler, J. Phys.: Condens. Matter **21**, 485404 (2009).
[8] *International Tables for Crystallography*, edited by T. Hahn (Springer-Verlag, Berlin, New York, 2005), Vol. A.
[9] X. Gonze and C. Lee, Phys. Rev. B **55**, 10355 (1997).
[10] S. Baroni, S. de Gironcoli, A. del Corso, and P. Gianozzi, Rev. Mod. Phys. **73**, 515 (2001).
[11] P. Umari, X. Gonze, and A. Pasquarello, Phys. Rev. B **69**, 235102 (2004).
[12] R. S. Mulliken, Phys. Rev. **43**, 279 (1933).
[13] D. Schwarzenbach, *Crystallography* (Wiley, Chichester, 1993).
[14] D. Royer and E. Dieulesaint, *Elastic Waves in Solids I* (Springer-Verlag, Berlin, New York, 2000).
[15] A. R. Goñi and K. Syassen, in *High Pressure in Semiconductor*

Physics I, edited by T. Suski and W. Paul (Academic Press, San Diego, London, New York, 1998).
[16] A. J. Bosman and E. E. Havinga, Phys. Rev. **129**, 1593 (1963).
[17] J. Shanker and S. Dixit, Phys. Status Solidi A **123**, 17 (1991).
[18] Ch. Kittel, *Introduction to Solid State Physics*, 8th ed. (Wiley, New York, 2005).
[19] S. de Gironcoli, *Phonons with density-functional perturbation theory*, documentation of the QUANTUM-ESPRESSO project.
[20] S. M. Ho, Mater. Sci. Eng. **54**, 23 (1982).
[21] X. Zhao and D. Vanderbilt, Phys. Rev. B **65**, 075105 (2002).
[22] F. Detraux, Ph. Ghosez, and X. Gonze, Phys. Rev. Lett. **81**, 3297 (1998).
[23] C. Pecharromán, M. Ocaña, and C. J. Serna, J. Appl. Phys. **80**, 3479 (1996).
[24] D. W. Liu, C. H. Perry, A. A. Feinberg, and R. Currat, Phys. Rev. B **36**, 9212 (1987).
[25] J. Cai, C. Raptis, Y. S. Raptis, and E. Anastassakis, Phys. Rev. B **51**, 201 (1995).
[26] A. Sekulić, K. Furić, and M. Stubičar, J. Mol. Struct. **410-411**, 275 (1997).
[27] G. Morell, R. S. Katiyar, D. Torres, S. E. Paje, and J. Llopis, J. Appl. Phys. **81**, 2830 (1997).
[28] J. M. Calderon-Moreno and M. Yoshimura, Solid State Ionics **154-155**, 125 (2002).
[29] I. A. Izyumov and V. N. Syromyatnikov, *Phase Transitions and Crystal Symmetry* (Kluwer Academic, Dordrecht, 1990).
[30] M. S. Dresselhaus, G. Dresselhaus, and A. Jorio, *Group Theory-Application to the Physics of Condensed Matter* (Springer-Verlag, Berlin, 2008).
[31] N. M. Balzaretti and J. A. H. da Jornada, Phys. Rev. B **52**, 9266 (1995).
[32] H. Mueller, Phys. Rev. **47**, 947 (1935).
[33] R. E. Cohen, M. J. Mehl, and L. L. Boyer, Physica B **150**, 1 (1988).
[34] A. P. Mirgorodsky, M. B. Smirnov, and P. E. Quintard, Phys. Rev. B **55**, 19 (1997).
[35] A. P. Mirgorodsky and P. E. Quintard, J. Am. Ceram. Soc. **82**, 3121 (1999).
[36] S. Fabris, A. T. Paxton, and M. W. Finnis, Phys. Rev. B **61**, 6617 (2000).
[37] G. Fadda, L. Colombo, and G. Zanzotto, Phys. Rev. B **79**, 214102 (2009).
[38] Th. Merle, R. Guinebretiere, A. Mirgorodsky, and P. Quintard, Phys. Rev. B **65**, 144302 (2002).
[39] P. Bouvier and G. Lucazeau, J. Phys. Chem. Solids **61**, 569 (2000).
[40] N. Kjerulf-Jensen, R. W. Berg, and F. W. Poulsen, in *Proceedings of the Second European Solid Oxide Fuel Cell Forum*, edited by B. Thorstensen (European Fuel Cell Forum, Switzerland, 1996).
[41] V. Lughi and D. R. Clarke, J. Appl. Phys. **101**, 053524 (2007).
[42] A. C. Lasaga and R. T. Cygan, Am. Mineral. **67**, 328 (1982).
[43] H. Zhang, Y. Liu, K. Zhu, G. Siu, Y. Xiong, and C. Xiong, J. Phys.: Condens. Matter **11**, 2035 (1999).
[44] A. Feinberg and C. H. Perry, J. Phys. Chem. Solids **42**, 513 (1981).
[45] M. Ishigame and T. Sakurai, J. Am. Ceram. Soc. **60**, 367 (1977).
[46] L. Shi, K.-C. Tin, and N.-B. Wong, J. Mater. Sci. **34**, 3367 (1999).
[47] R. Terki, G. Bertrand, H. Aourag, and C. Coddet, Mater. Sci. Semicond. Process. **9**, 1006 (2006).
[48] J. Haines, J. M. Léger, S. Hull, J. P. Petitet, A. S. Pereira, C. A. Perottoni, and J. A. H. da Jornada, J. Am. Ceram. Soc. **80**, 1910 (1997).
[49] D. Porezag and M. R. Pederson, Phys. Rev. B **54**, 7830 (1996).
[50] M. Veithen, X. Gonze, and Ph. Ghosez, Phys. Rev. B **71**, 125107 (2005).
[51] E. Fernández López, V. Sánchez Escribano, M. Panizza, M. M. Carnasciali, and G. Busca, J. Mater. Chem. **11**, 1891 (2001).
[52] M. Li, Z. Feng, G. Xiong, P. Ying, Q. Xin, and C. Li, J. Phys. Chem. B **105**, 8107 (2001).
[53] J.-L. You, G.-C. Jiang, S.-H. Yang, J.-C. Ma, and K.-D. Xu, Chin. Phys. Lett. **18**, 991 (2000).
[54] S. N. Tkachev, M. H. Manghnani, A. Niilisk, J. Aarik, and H. Mändar, Spectrochim. Acta, Part A **61**, 2434 (2005).